



# Porphyrins Through the Looking Glass: Spectroscopic and Mechanistic Insights in Supramolecular Chirogenesis of New Self-Assembled Porphyrin Derivatives

Manuela Stefanelli<sup>1†</sup>, Marco Savioli<sup>1†</sup>, Francesca Zurlo<sup>1</sup>, Gabriele Magna<sup>1</sup>, Sandra Belviso<sup>2</sup>, Giulia Marsico<sup>2</sup>, Stefano Superchi<sup>2</sup>, Mariano Venanzi<sup>1</sup>, Corrado Di Natale<sup>3</sup>, Roberto Paolesse<sup>1</sup> and Donato Monti<sup>1,4\*</sup>

## OPEN ACCESS

### Edited by:

Victor Borovkov,  
South-Central University for  
Nationalities, China

### Reviewed by:

Minghua Liu,  
Institute of Chemistry (CAS), China  
Michiya Fujiki,  
Nara Institute of Science and  
Technology (NAIST), Japan  
Roberto Purrello,  
University of Catania, Italy

### \*Correspondence:

Donato Monti  
monti@stc.uniroma2.it  
donato.monti@uniroma2.it

<sup>†</sup>These authors have contributed  
equally to this work

### Specialty section:

This article was submitted to  
Supramolecular Chemistry,  
a section of the journal  
Frontiers in Chemistry

Received: 27 July 2020

Accepted: 09 September 2020

Published: 15 October 2020

### Citation:

Stefanelli M, Savioli M, Zurlo F,  
Magna G, Belviso S, Marsico G,  
Superchi S, Venanzi M, Di Natale C,  
Paolesse R and Monti D (2020)  
Porphyrins Through the Looking  
Glass: Spectroscopic and Mechanistic  
Insights in Supramolecular  
Chirogenesis of New Self-Assembled  
Porphyrin Derivatives.  
Front. Chem. 8:587842.  
doi: 10.3389/fchem.2020.587842

<sup>1</sup> Department of Science and Chemical Technologies, University of Rome "Tor Vergata", Rome, Italy, <sup>2</sup> Department of Sciences, University of Basilicata, Potenza, Italy, <sup>3</sup> Department of Electronic Engineering, University of Rome Tor Vergata, Rome, Italy, <sup>4</sup> Department of Chemistry, University La Sapienza, Rome, Italy

The solvent driven aggregation of porphyrin derivatives, covalently linked to a L- or D-prolinate enantiomer, results in the stereospecific formation of species featuring remarkable supramolecular chirality, as a consequence of reading and amplification of the stereochemical information stored in the proline-appended group. Spectroscopic, kinetic, and topographic SEM studies gave important information on the aggregation processes, and on the structures of the final chiral architectures. The results obtained may be the seeds for the construction of stereoselective sensors aiming at the detection, for example, of novel emergent pollutants from agrochemical, food, and pharmaceutical industry.

**Keywords:** porphyrins, circular dichroism, supramolecular chemistry, supramolecular chirogenesis, self-assembly, chirality

## INTRODUCTION

Porphyrin-based chiral supramolecular systems are of great importance owing to their potential application in wide fields of science and technology (Cui et al., 2015; Paolesse et al., 2017; Lee et al., 2018), and for the implication on the emergence of homochirality in Life (Guijarro and Yus, 2009). Addressed protocols pursued for the formation of such a species usually rely on the use of either chiral or achiral platforms (Monti, 2014; Liu et al., 2015; Magna et al., 2019). In the former case, the stereochemical course of the self-assembling process is governed by the presence of chiral groups linked on the porphyrin peripheral frame (Oliveira-González et al., 2015; van der Weegen et al., 2017). In the latter issue, final chiral suprastructures are obtained by interaction of achiral substrates with external physical effectors, such as hydrodynamic directional forces (Sorrenti et al., 2012; Arteaga et al., 2016); magnetic fields (Micali et al., 2012); LB and LS techniques (Chen et al., 2011), or chiral molecular templates, such as surfactants (El-Hachemi et al., 2008), chiral polymeric matrices (D'Urso et al., 2012), chiral ligands (Borovkov and Inoue, 2006; Berova et al., 2007) or carboxylic acids (Castriciano et al., 2011). With this regard, Monsù Scolaro showed that the assembly of a non-chiral porphyrin derivative templated by the two different enantiomers of tartaric acid proceeds

with different kinetics and results in final chiral suprastructures with highly different anisotropy factors, which are strictly dependent on the enantiomer used as a templating agent (Castriciano et al., 2012). These findings indicate the complexity of factors that play a crucial role in the formation of such chiral species. As a part of our studies dedicated to the construction of chiral porphyrin aggregates (Monti et al., 2010; Zelenka et al., 2011), we investigated the self-assembly behavior of intrinsically chiral zinc-tetraphenylporphyrin derivatives, characterized by the presence of covalently linked enantiomers of L- or D-prolinate groups on the molecular frame (**Scheme 1**). The molecular information stored on the periphery of the macrocycles, besides inferring key amphiphilic properties to the monomers, can be effectively read out during the self-assembly of the aromatic platforms, once steered by hydrophobic effect, owing to the conformational rigidity, and robustness toward adventitiously caused racemization of the prolinate residues. This, in certain aspects, unique aminoacid has been recently found to play a role in asymmetric aminocatalysis (Mathew et al., 2004). We may anticipate that the process follows a highly stereospecific multistep mechanism, to give assemblies with specular CD features, indicating the formation of aggregate structures with opposite supramolecular chirality, dictated by the type of stereocenter present on the macrocycle. Further kinetic and topographic SEM investigations gave clear cut insights on the mechanism and the morphology of the chiral supramolecular structures formed. The results obtained are of great importance for the fabrication of sensors featuring stereoselective properties. We recently found, for example, that hybrid organic-inorganic materials, constituted by ZnO nanoparticles covalently linked to a porphyrin enantiomer studied in detail in the present work, are able to selectively detect the different enantiomers of chiral analytes, such as limonene and other terpenes (Stefanelli et al., 2019).

## RESULTS AND DISCUSSION

### Synthesis of Porphyrin Derivatives

Synthesis of the title porphyrins has been accomplished by following the path reported in **Scheme 1**, which relies on straightforward procedures used in peptide chemistry. As a first stage, the 5-(4-carboxyphenyl)-10,15,20-triphenylporphyrin **pCTPP** was reacted with (L)- or (D)-proline *tert*-butyl ester using the EDCl/HOBT coupling reagents, providing the corresponding prolinate derivatives which were subsequently hydrolyzed in a TFA/CH<sub>2</sub>Cl<sub>2</sub> mixture to give the amphiphilic compounds (L)**H<sub>2</sub>P**(-) and (D)**H<sub>2</sub>P**(-). The further metalation with an excess of zinc acetate in CHCl<sub>3</sub>/MeOH afforded the corresponding (L)**ZnP**(-) and (D)**ZnP**(-) complexes (Stefanelli et al., 2019).

### Aggregation Studies

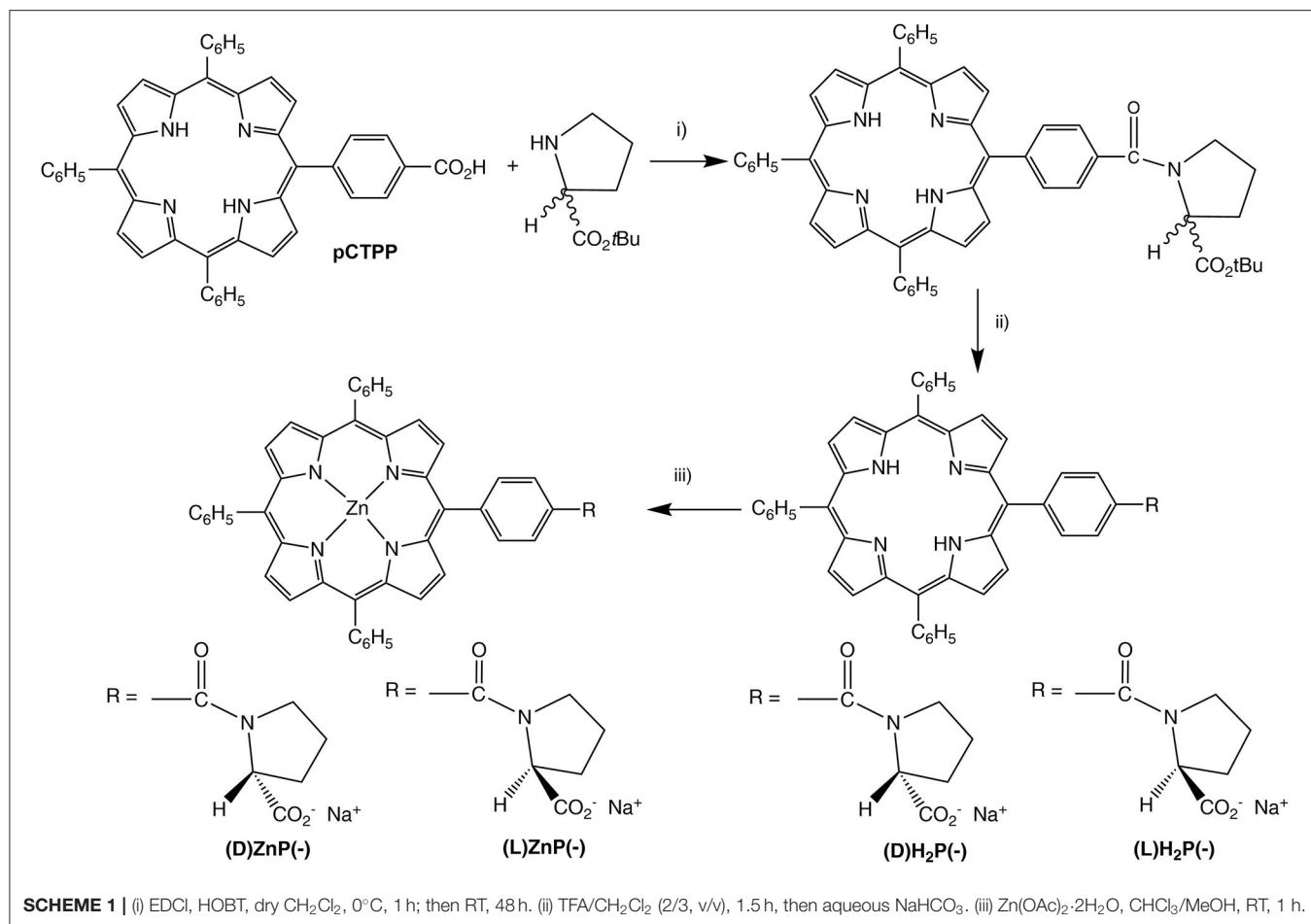
#### Spectroscopic Investigations

Aggregation of title porphyrins has been carried out in aqueous ethanol solutions (EtOH/H<sub>2</sub>O 25:75 v:v; 298 K) typically at 5 μM concentration, by strictly following a “porphyrin first” protocol, as reported in the Experimental Section. Previously published studies, carried out by our group and by others,

pointed out the strong dependence of the aggregation process on the experimental conditions, such as the order in which the reagents are mixed (Micali et al., 2000). Moreover, the chiral induction exerted by homochiral dopants can be effectively modulated during the early milliseconds mixing stage (i.e., standard flask preparation vs. microfluidic mixing; Sorrenti et al., 2016). However, within the standard playground of solutions preparation, the peculiar solvent mixture used allows for a good reproducibility of the results and a convenient time of reaction, to be followed by conventional spectroscopic techniques. It is important to remark that the preparation of the samples requires also an additional step of sonication and microfiltration of the solutions, to ensure an optimal reproducibility of the results obtained, in terms of spectral features (UV-Vis and CD band intensities) and kinetic parameters (for a brief discussion see **Supplementary Material**). Sonication steps have been demonstrated to feature a key role in supramolecular chirogenesis of porphyrin macrocycles and related structures (Liu et al., 2015; El-Hachemi et al., 2016). The protocol followed is described in full details in the Experimental Section.

In ethanol, the title amphiphilic macrocycles are in monomeric form ( $\lambda_{\text{max}} = 424 \text{ nm}$ ; **Figure 1A**, trace a); the addition of a proper amount of water steers the self-aggregation process driven by hydrophobic effect, as indicated by the typical UV-Vis spectral changes (**Figure 1A**, trace b), which is complete within the time of mixing, likely driven by  $\pi$ - $\pi$  interactions (Type-I aggregates). The corresponding spectral pattern indicates a hypochromic effect with a concomitant broadening and small red-shift of the Soret B band to 427 nm. CD spectroscopy reveals that these species feature, although of low intensities, appreciable supramolecular chirality of opposite sign, depending on the configuration of the appended groups. In particular, the aggregates of (D)**ZnP**(-) show a positive (+/-) bisignate spectrum, whereas those of the (L)**ZnP**(-) enantiomer show a mirrored, negative pattern (-/+), as reported in **Figure 2A**. The reproducibility of the results, along with the specularity of the dichroic bands, safely rules out any effect due to the presence of adventitious chiral residues in the medium (El-Hachemi et al., 2009), also upon using of distilled water from different sources and time of storage. Interestingly, these species show a further slow evolution, which is generally completed within few weeks, into structures of different morphology (Type-II aggregates; **Figure 1A**, trace c). Accordingly, the UV-Vis spectra of the solutions show a further slow decrease of intensity of the Soret bands, evolving at final equilibrium into a double peaked coupled B band ( $\lambda_{\text{max}} = 422$  and 443 nm) in the case of both (L)**ZnP**(-) and its (D)**ZnP**(-) stereoisomer, with a clear isosbestic point at 439 nm (**Figure 1B**).

Again, CD experiments gave insights on this phenomenon. In the cases of both of the enantiomers, the spectra show remarkable evolution of the initial features, with the gradual formation of multi-patterned coupled bands featuring intensities increased by two order of magnitude, with crossover points in correspondence of the UV-Vis absorption maxima (**Figure 2B,C**). This complex pattern has been ascribed to the formation of J-type aggregates of complex morphology, with excitonic coupling along two preferential space directions (Ohno et al., 1993). In particular, the



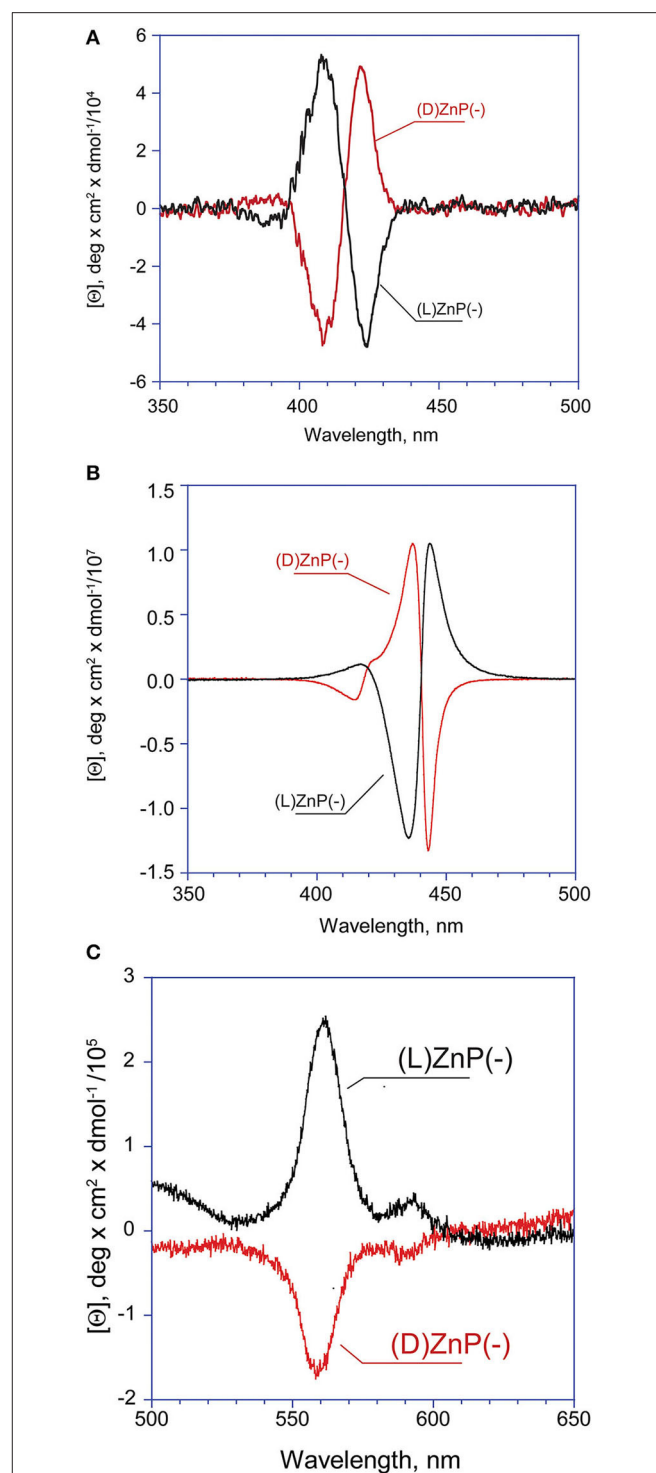
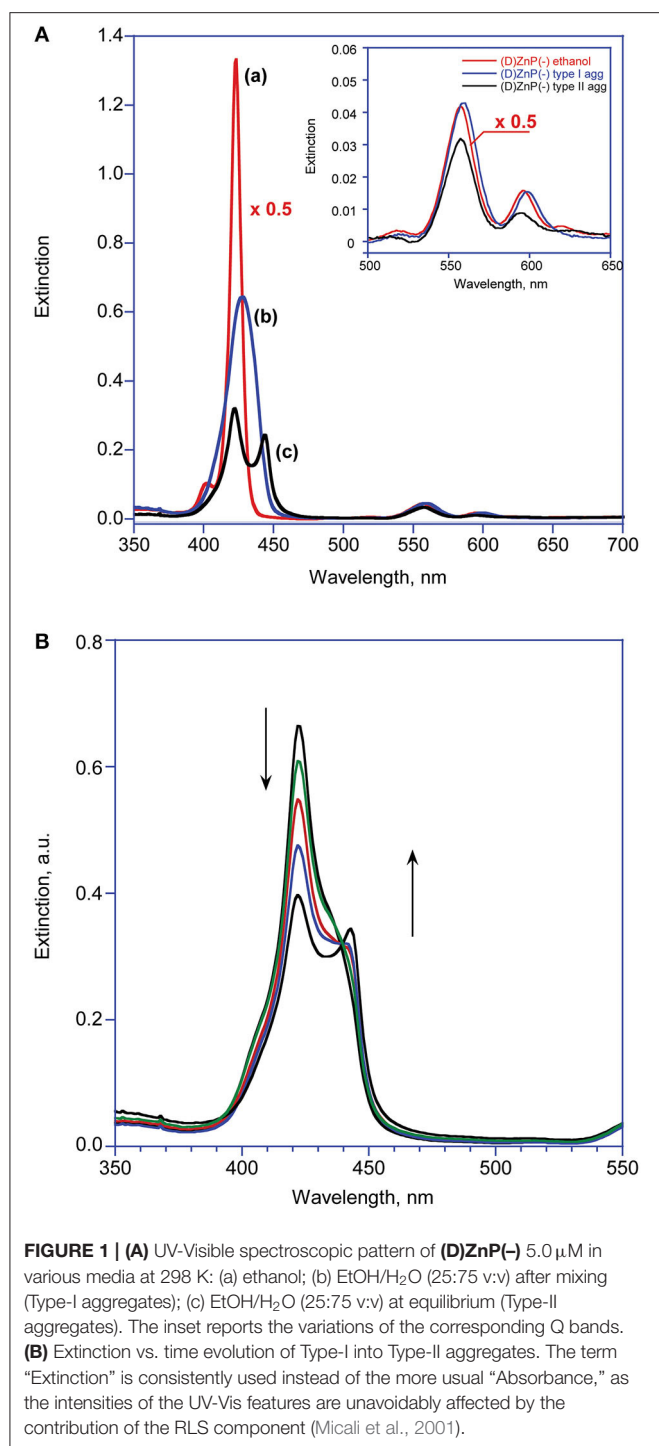
supramolecular structures derived from the **(L)ZnP(-)** species, show a  $+/-/+$  pattern, while those of the **(D)ZnP(-)** forms show a specular  $-/+/-$  sign. Accordingly, the calculated anisotropy factors  $g$  (Berova et al., 2000) are  $9.5 (\pm 0.5) \times 10^{-5}$  for both the initial (Type-I) aggregates;  $0.068 (\pm 0.005)$  and  $0.071 (\pm 0.008)$  for **(L)ZnP(-)** and **(D)ZnP(-)** respectively, at equilibrium (Type-II species;  $5 \mu\text{M}$  initial concentration). These values indicate an enhancement of the intrinsic chirality on going to the larger, more structured Type-II species.

Accordingly, Type-II aggregates showed quenching of fluorescence emission (**Supplementary Figure 1A**), and intense Resonance Light Scattering features (**Supplementary Figures 1B,C**), as a consequence of an efficient delocalization of porphyrin exciton momenta over a large number of electronically coupled monomers, with respect to those featured in the first aggregation stage, indicating the formation of larger and strongly coupled self-assembled structures (Pasternack et al., 1993). Finally, the corresponding excitation spectra, carried out at both the emission wavelength maxima (i.e., at 604 or 650 nm) gave the exact reproduction of the UV-Vis Type-II spectral pattern, ruling out the formation of distinct families of H and J aggregates

(**Supplementary Figure 1D**). The supramolecular structures formed at  $10 \mu\text{M}$  concentration featured a somewhat reduced  $g$ -value to about  $0.049 (\pm 0.006)$ , indicating a lesser degree of order of the final structures. Analogous and even more dramatic effect, has been previously reported (Romeo et al., 2014), pointing out the importance of the initial nucleation stage preceding the ordered growth of final structures.

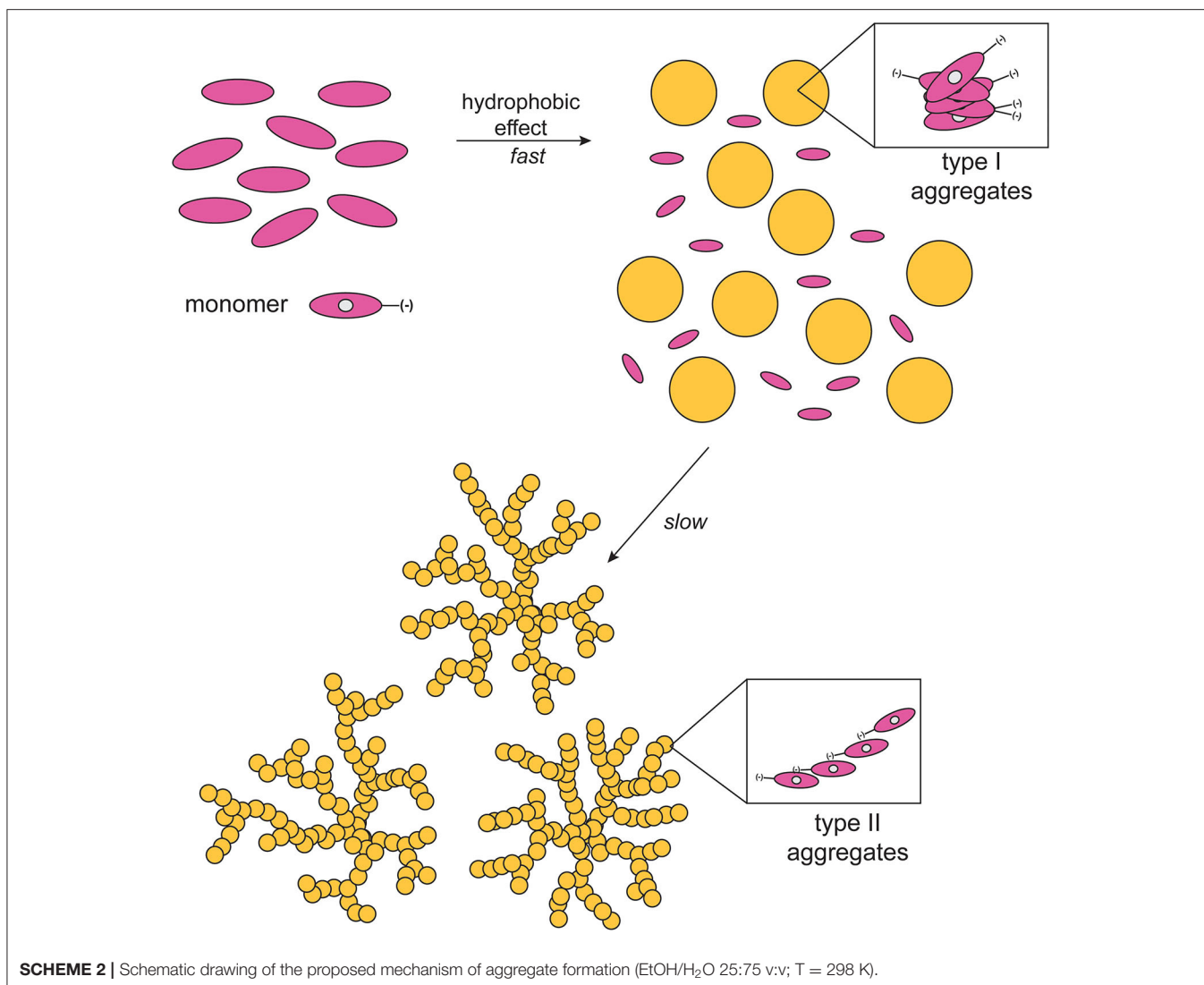
The results obtained showed good reproducibility well within a factor of two, also with porphyrins from different synthetic batches, although a strong decrease of the overall CD spectral intensities of the aggregates is generally observed when aged porphyrins stock solutions are used (time of storage longer than 1 month). Conversely, studies carried out at  $1 \mu\text{M}$  concentration did not give evidences of complete formation of Type-II chiral aggregates, resulting in corresponding dichroic bands of very low intensity, which in some cases were difficult to be disentangled from the background noise. Prolonged standing of these solutions merely resulted in the flocculation of uncharacterized material.

It should be emphasized that in all of the cases observed the final CD spectra feature a sign inversion of the main lower energy bands, with respect to the blue-shifted coupled pattern. Inversion of these J-band has been also found by others in



the case of the formation of chiral porphyrin aggregates upon symmetry breaking induced by rotary evaporation (Sorrenti et al., 2012), and has been ascribed to a distortion from the planarity of the macrocycles due to steric hindrance. Similar results have been reported by Micali and Monsù Scolaro (Micali et al., 2006), for the case of chiral fractal structures of a water-soluble tetrakis(*p*-sulphonatophenyl)porphyrin derivative,

assembled in the presence of D- and L-tartaric acid as chiral effectors. In the present case, this effect may arise from a coordination of the Zn ion by the proline carboxylate



group, and this event would likely constitute the driving force for the evolution toward the final Type-II species. The involvement of Zn-coordination is also suggested by the fact that the free-base analogs of the title porphyrins [(D)- and (L)H<sub>2</sub>P(-); **Scheme 1**] show different aggregation behavior with different CD spectral features, which are composed by simple mirrored bisignated bands, with constant intensity and pattern throughout the whole temporal window examined and, relevantly, with same signs of that of the Type-I species (**Supplementary Figure 2**). As far as the macrocycles intimate molecular level structure is concerned, a metastable mutual *syn* configuration for the Type-I aggregates, and a thermodynamically stable extended *anti* configuration could be proposed. This suggestion was made on the basis of strong similarities of both Soret band and CD profiles of the aggregates to those of chiral *syn*- or *anti*-geometry of bis-(Zn)porphyrin derivatives with several chiral ligands (Borovkov et al., 2000, 2001). A pictorial representation of the mechanism is reported in **Scheme 2**. Furthermore, if the aggregation of

the title Zn porphyrins is carried out in the presence of an excess of benzylamine, a competing achiral nitrogen ligand, the aggregation occurs with the formation of final achiral, CD silent, aggregate structures (results not shown), confirming the key role of the coordination on the formation of the final structures.

As far as the overall aggregation process is concerned, we recently found an analogous two-step process in the aggregation of related cationic L-proline-porphyrin derivatives in analogous aqueous media (Lorecchio et al., 2014; Caroleo et al., 2019), and also in the study of the interaction of a chiral Zn-porphyrin derivative with chiral anionic surfactants in water, that results in the rapid formation of small sized aggregates, followed by a slower step in which the initial species rearrange in more ordered and specific structures driven by Zn-coordination (Simoncini et al., 2014). Same phenomenon has been also observed by others in organic solvent (Feldborg et al., 2011), in the case of water-soluble tetrapyrrolic macrocycles

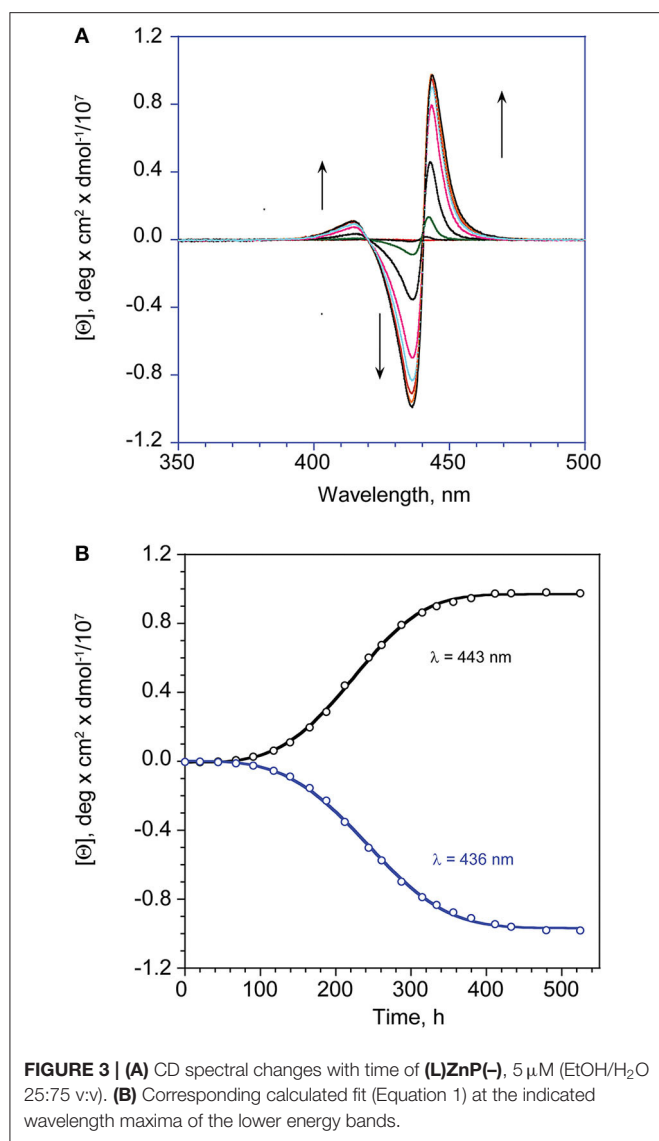


**FIGURE 3 | (A)** CD spectral changes with time of (L)ZnP(-), 5  $\mu$ M (EtOH/H<sub>2</sub>O 25:75 v/v). **(B)** Corresponding calculated fit (Equation 1) at the indicated wavelength maxima of the lower energy bands.

(El-Hachemi et al., 2016) or, amazingly, even in solid state (Borovkov et al., 2003).

Finally, when the aggregation experiment was carried out on the racemic mixture (i.e., 5  $\mu$ M of both the enantiomers) only a broadening and hypochromic effect of the Soret bands and silent CD spectra are obtained, indicating the formation of non-specific achiral structures, likely due to the mismatching of the chiral proline groups during the key molecular recognition event.

### Kinetic Studies

Kinetic studies, carried out on the slow formation step of Type-II aggregates, allowed to get more insights on the intimate mechanism of formation of such important chiral architectures. In all of the case examined, the kinetic profiles [i.e., molar ellipticity  $[\Theta]$  vs. time] followed a sigmoidal autocatalytic behavior (Figures 3A,B) that could be successfully modeled

by a “fractal-type” exponential equation (Equation 1) formerly developed by Pasternack et al. (2002) for the case of disassembly of porphyrin aggregates by cyclodextrins. The equation used is of the form:

$$[\Theta] = [\Theta]_{eq} + ([\Theta]_0 - [\Theta]_{eq})e^{\left[\frac{-(kt)^{n+1}}{(n+1)}\right]} \quad (1)$$

In this equation,  $[\Theta]$ ,  $[\Theta]_0$ , and  $[\Theta]_{eq}$  are the molar ellipticity values at time  $t$ , time = 0, and at equilibrium, respectively;  $n$  is the “aggregate growth rate” parameter, and  $k$  the kinetic constant. We consistently found values of  $n > 1$ , indicating that the interaction between monomers and the growing structures become increasingly favored with time, i.e., with the increase of their surface area.

It is worthwhile of noting that this equation is a reduced form of a more general non-conventional equation previously developed by Pasternack himself (Pasternack et al., 2000), employed in the kinetic studies of fractal growth of porphyrin aggregates onto DNAs. This latter equation includes, beside a kinetic constant for an uncatalyzed path ( $k_0$ ), a further parameter ( $m$ ) related to the number of monomers forming the aggregation nuclei with catalytic activity (nucleation seeds). The equation reduces to Equation 1 in the case of  $m = 1$ , implying that the rate-determining step is the adhesion of the monomer to the growing assemblies, and not the formation of catalytically-active nucleation seeds. In our case the initial oligo-assemblies formed (Type-I species) should act as *single-site enantiomorphous surfaces* (i.e., a collection of uniform and independent chiral interaction sites), that promote the catalyzed growth of the final suprastructures with high stereospecificity. The legitimacy of this hypothesis is corroborated by the fact that the fit of the experimental values with the original “full-form equation” always gave  $m$ -values very close to 1 (i.e., from 0.95 to 1.1  $\pm$  0.2) and negligible values of  $k_0$  that faded within their experimental errors, along with a lower adherence to the experimental data points and higher uncertainties of the obtained kinetic parameters. The results have been reported in Table 1.

From the inspection of the table, the second step kinetic constant has been found to be in the order of  $10^{-4} \text{ min}^{-1}$  for the process carried out at 5  $\mu$ M, for both of the enantiomers, with  $n$ -values of *ca* 2 (entry 1). Kinetic experiments carried out at 10  $\mu$ M concentration resulted in an increase of the rate constant within one order of magnitude, along with an exponential growing factor of  $n = 4$  (entry 3), which should arise from both the increase of the number of the initial nucleation structures, and on their increased size (i.e., area of the catalytic surfaces). Same results, in good agreement within experimental errors, have been obtained by UV-Vis spectroscopy, by following the slow decay with time of the Soret band of the Type-I species (see Table 1, entry 2, and Supplementary Figure 3).

Interestingly, experiments carried out at 1  $\mu$ M concentration revealed that the formed aggregates featured very low supramolecular chirality. However, the lower aggregation rate observed at this concentration regime, allowed for shedding light on the initial fast aggregation stage (i.e., formation of Type-I molecular structures) by UV-Vis technique. Remarkably,

**TABLE 1** | Kinetic parameters for the aggregation reaction of (L)ZnP(-) and (D)ZnP(-) in EtOH/H<sub>2</sub>O (25:75 v:v; 298 K) at different concentrations.

Concentration, M	(L)ZnP(-)		(D)ZnP(-)	
	$k, \text{min}^{-1}$	$n$	$k, \text{min}^{-1}$	$n$
(1) $5.0 \times 10^{-6} \text{ M}^{(a)}$	$9.3 (\pm 0.8) \times 10^{-5}$	$2.3 \pm 0.7$	$9.0 (\pm 0.8) \times 10^{-5}$	$2.7 \pm 0.6$
(2) $5.0 \times 10^{-6} \text{ M}^{(b)}$	$9.7 (\pm 0.6) \times 10^{-5}$	$1.8 \pm 0.3$	$8.5 (\pm 0.4) \times 10^{-5}$	$1.7 \pm 0.2$
(3) $1.0 \times 10^{-5} \text{ M}^{(a)}$	$8.4 (\pm 0.7) \times 10^{-4}$	$4.8 \pm 0.9$	$7.3 (\pm 0.6) \times 10^{-4}$	$4.0 \pm 0.6$
(4) $1.0 \times 10^{-6} \text{ M}^{(c)}$	$6.0 (\pm 0.5) \times 10^{-2}$	$0.12 \pm 0.05$	$5.0 (\pm 0.4) \times 10^{-2}$	$0.11 \pm 0.03$

(a) Followed by CD spectroscopy, fitted by Equation 1; (b) Followed by UV-Vis spectroscopy ( $\lambda = 423 \text{ nm}$ ), fitted by Equation 1; (c) Followed by UV-Vis spectroscopy ( $\lambda = 422 \text{ nm}$ ), fitted by Equation 2.

the extinction vs. time plot revealed a Diffusion Limited Cluster-Cluster Aggregation kinetic (DLCCA; **Figure 4**), which entails the rapid formation of small clusters, that subsequently slowly stick together forming larger structures (Monsù Scolaro et al., 2002). The equation used is of the form

$$[E] = [E]_o + ([E]_{eq} - [E]_o)(1 - e^{(-kt)^n}) \quad (2)$$

where  $E$  is the extinction values of the Soret band of the monomeric forms ( $\lambda = 424 \text{ nm}$ ) at time  $t$ , at time  $t = 0$  and at equilibrium, respectively;  $k$  is the apparent first-order reaction constant, and  $n$ , the so called “stretching factor,” modulates the diffusion growth of the aggregates, which in the case of this observed mechanism is strictly required to be  $n < 1$ . Due to the fast decay of the Soret intensity, the value at time  $t = 0$  is calculated in the closest non-aggregative conditions (EtOH/H<sub>2</sub>O 50% v:v).

The corresponding fit gave an estimation of the calculated rate constant values in the order of  $10^{-2} \text{ min}^{-1}$ , whereas the  $n$ -values are about 0.1 for both (L)ZnP(-) and (D)ZnP(-) (entry 4, **Table 1**).

## Topographic SEM Investigations

The structural features of the supramolecular species, have been investigated by Scanning Electron Microscopy (SEM) of drop-casted equilibrium solutions. Micrographies show the formation of regular finely branched fractal structures of about 5–10  $\mu\text{m}$  of diameter, throughout the surface investigated, for both the (L)ZnP(-) and (D)ZnP(-) derivatives (**Figures 5A–C**), in agreement with the peculiar kinetic process found for the formation of these supramolecular self-assembled chiral structures. Interestingly, racemic mixtures resulted in the formation of small globular structure only (**Figure 5D**), according to the negligible stereospecificity of the supramolecular assemblies. We previously found in fact that, in peptide self-assembly, globular structures predominate when the process is driven by non-specific interactions (e.g., hydrophobic effect). Where specific interactions between ordered structures predominate, the formation of fibrillar structures is then observed (Caruso et al., 2013).

## CONCLUSIONS AND FUTURE PERSPECTIVES

In summary, the self-assembly process of amphiphilic porphyrin derivatives, functionalized by the two different stereoisomers

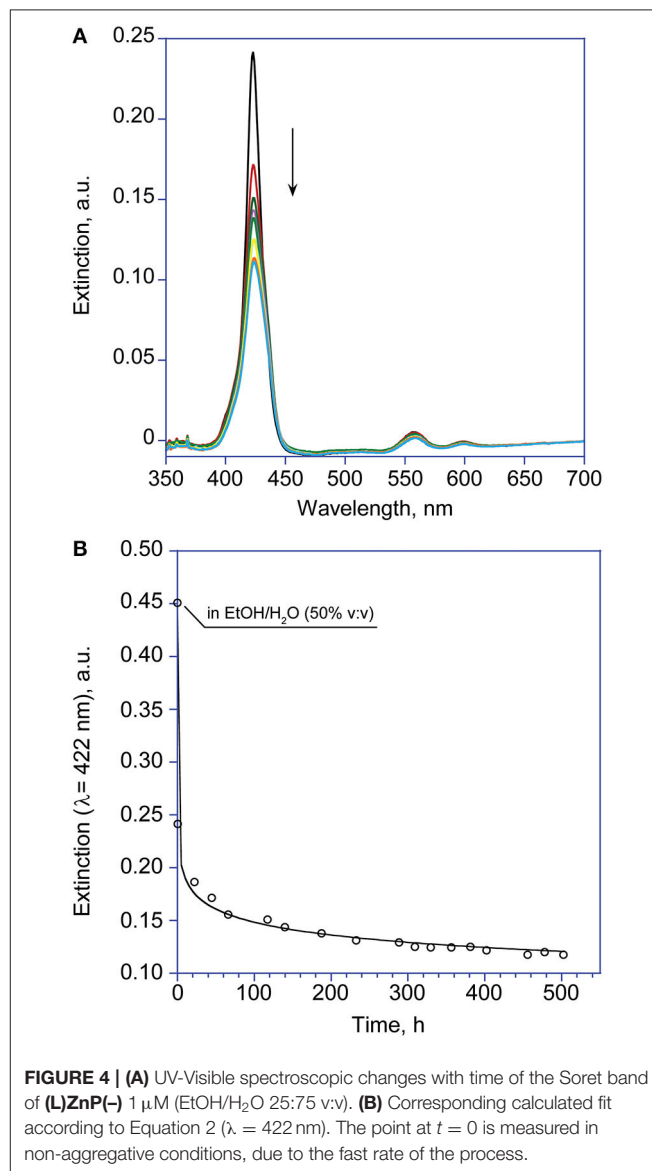


**FIGURE 4** | (A) UV-Visible spectroscopic changes with time of the Soret band of (L)ZnP(-) 1  $\mu\text{M}$  (EtOH/H<sub>2</sub>O 25:75 v:v). (B) Corresponding calculated fit according to Equation 2 ( $\lambda = 422 \text{ nm}$ ). The point at  $t = 0$  is measured in non-aggregative conditions, due to the fast rate of the process.

of proline, results in fractal architectures featuring specular chiroptical properties, and alike morphology. Combined spectroscopic and kinetic studies pointed out the occurrence of a two-step process, in which an initial fast and chaotic assembly is followed by a slower stereospecific growth of fractal

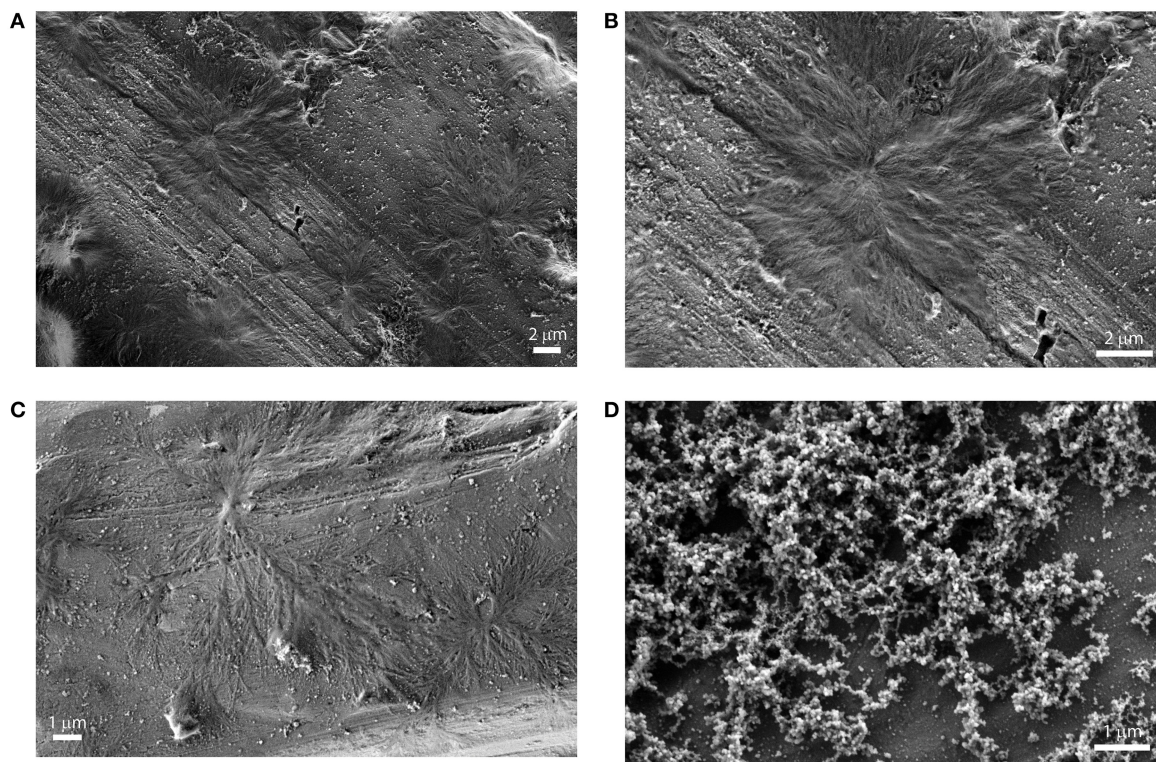


**FIGURE 5** | SEM images of drop casted equilibrium solutions of porphyrin aggregates ( $5 \mu\text{M}$  (EtOH/ $\text{H}_2\text{O}$  25:75 v:v). (A): (L)ZnP(-); (B): (L)ZnP(-) enlargement of 5A; (C): (D)ZnP(-); (D) racemic mixture.

architectures, featuring intense coupled CD bands. Careful choice of experimental conditions gave a good control on the spectroscopic and morphological features of the final species. Detailed Scanning Electron Microscopy studies confirmed the complex peculiar structures of the obtained species. These findings would be of importance for understanding the fundamental process of evolution of homochirality at biological level (Guijarro and Yus, 2009), and for the development of chiral materials that, coupled with nanotechnology, constitutes a deeply pursued target with a wide range of exploitation in many important areas such as catalysis (Yoon et al., 2012), non-linear optics (Valev et al., 2014), materials science (Wang et al., 2013), sensors (Paolesse et al., 2011; Labuta et al., 2015; Intrieri et al., 2018), and catalysis (Zhou et al., 2018).

## EXPERIMENTAL SECTION

### General

Reagents and solvents were of commercial sources, in the highest degree of purity and were used as received. (D)-proline *tert*-butyl ester was purchased from Chem Impex International, Inc (USA). Thin-layer chromatography (TLC) was performed on Merck silica gel plates. Chromatographic purification on column was accomplished by using silica gel 60 (70–230 mesh, Sigma Aldrich) as the stationary phase.  $^1\text{H}$  NMR spectra of the new porphyrin derivatives (D) $\text{H}_2\text{P}(-)$  and (D)ZnP(-) were recorded

with a Bruker AV300 spectrometer (300 MHz) in  $\text{CDCl}_3$  and  $\text{THF-d}_8$  and are internally referenced to residual proton solvent signals ( $\text{CDCl}_3$ :  $\delta = 7.24$  ppm,  $\text{THF-d}_8$ :  $\delta = 1.73$  and 3.58 ppm). FAB mass spectra were obtained with a VG-Quattro spectrometer in the positive-ion mode by using  $\text{CHCl}_3$  as the solvent and *m*-nitrobenzyl alcohol (Sigma Aldrich) as the matrix. Solvents used for spectroscopic measurements were of spectroscopic grade. UV/Vis spectra were recorded on a Cary 100 spectrophotometer.

CD spectra were performed on a JASCO J-1500, equipped with a thermostated cell holder set at 298 K, and purged with ultra-pure nitrogen gas. Linear Dichroism contribution (LD) has been found to be in all of the cases examined  $< 0.0004$  DOD units, in all of the case examined. Fluorescence emission and Resonance Light Scattering measurements were performed on a Fluoromax-4 (HORIBA Scientific) spectrofluorimeter, in a synchronous scan mode, in which the emission and excitation monochromators are pre-set to identical wavelengths. Microstructural analysis of (D)- and (L)- porphyrin aggregates was carried out by using a Field Emission Scanning Electron Microscope FE-SEM, SUPRATM 35, Carl Zeiss SMT, Oberkochen, Germany. Samples have been prepared by slow evaporation of  $20 \mu\text{L}$  of the proper solution, on a previously cleaned aluminum stub ( $\text{MeOH}$ ;  $\text{N}_2$  flow). Sonication of the prepared solutions have been performed by ultrasound thermostath Fisher Scientific FB 15047, 90 W power supply, ultrasonic frequency of 37 kHz. Chiral HPLC analyses were performed

with a JASCO PU-1580 intelligent HPLC pump equipped with a Rheodyne model 7725i 20  $\mu\text{L}$  injector and coupled with a Varian 2,550 UV detector. Data were collected by using the Borwin software (Jasco, Japan). The Lux i-Amylose-1 [amylose tris(3,5-dimethylphenylcarbamate)] chiral chromatographic column (250 mm  $\times$  4.6 mm I.D., 5  $\mu\text{m}$  particle size) was purchased from Phenomenex (Torrance, CA, USA). HPLC runs were performed eluting with a mixture *n*-Hexane:EtOH (80:20, v/v) at flow rates of 0.7 mL  $\text{min}^{-1}$  and monitoring by UV detection at 350 nm. Samples were dissolved in the eluent, briefly sonicated, and filtered through a 0.45  $\mu\text{m}$  membrane (Whatman, UK) prior to injection.

## Synthesis and Characterization of Porphyrin Derivatives

The chiral porphyrin derivatives investigated were prepared as outlined in **Scheme 1**. The synthesis and characterization of the (L)-prolinated porphyrins was recently reported (Stefanelli et al., 2019). Thus, herein we report the experimental details to prepare the (D)- counterpart. As expected, the spectroscopic characterization of these new compounds is fully in agreement with those just reported for the corresponding (L)-analogs.

### Synthesis of (D) $\text{H}_2\text{P}(-)$

To a stirred solution of 5-(4-carboxyphenyl)-10,15,20-triphenylporphyrin (**pCTPP**) (104 mg, 0.158 mmol) in dry  $\text{CH}_2\text{Cl}_2$  (25 mL) kept at 0°C, 1-ethyl-3-(3-dimethylaminopropyl)carbodiimide hydrochloride (EDCI) (30 mg, 0.156 mmol), hydroxybenzotriazole (HOBT) (22 mg, 0.162 mmol) and *N*-methylmorpholine (82  $\mu\text{L}$ , 0.746 mmol) were added. The resulting solution was stirred under  $\text{N}_2$  for 1 h, then (D)-proline *tert*-butyl ester (97  $\mu\text{L}$ , 0.474 mmol) was added. The ice bath was removed and the reaction was allowed to reach the room temperature, then stirred for 48 h. Afterwards, the solvent was evaporated and the reaction crude was dissolved in chloroform and washed with brine (3  $\times$  100 mL). The organic phases were collected, dried over anhydrous  $\text{Na}_2\text{SO}_4$  and then purified on silica chromatographic column, eluting with  $\text{CHCl}_3$ . In a second step, the obtained porphyrin was dissolved in TFA/ $\text{CH}_2\text{Cl}_2$  mixture (2/3 v/v; 25 mL). The reaction was stirred at room temperature for 1.5 h. After the solvent removal under reduced pressure, the green residue was dissolved in  $\text{CHCl}_3$  and neutralized with a saturated solution of  $\text{NaHCO}_3$ . The organic phase was dried over  $\text{Na}_2\text{SO}_4$ , concentrated and crystallized by adding an equal volume of *n*-pentane. Porphyrin was obtained as bright purple crystals (81 mg, 0.107 mmol; 68% yield). UV-Vis ( $\text{CHCl}_3$ ):  $\lambda_{\text{max}}$  ( $\epsilon$ ,  $\text{M}^{-1} \text{cm}^{-1}$ ) = 419 (125,900), 515 (6,310), 547 (6,290), 585 (5,010), 640 (3,160) nm.  $^1\text{H}$  NMR (300 MHz,  $\text{CDCl}_3$ ): 8.80 (br s, 8 H,  $\beta$ -pyrr), 8.19 (m, 4H, ArH), 8.17 (m, 6H, ArH), 7.71 (m, 3H, ArH), 7.60 (m, 6H, ArH), 4.5 (m, 1 H, proline  $\alpha$ -H), 3.97 (m, 2 H, proline  $\delta$ -H), 2.44 (m, 2 H, proline  $\beta$ -H), 2.07 (m, 2 H, proline  $\gamma$ -H), -2.79 (s, 2H, NH). FAB-MS (NBA), *m/z*: 756  $[\text{M}]^+$ .

### Synthesis of (D) $\text{ZnP}(-)$

To a stirred solution of porphyrin (D) $\text{H}_2\text{P}(-)$  (90 mg, 0.119 mmol) dissolved in  $\text{CHCl}_3$  (15 mL) an excess of a methanolic

solution of  $\text{Zn}(\text{OAc})_2 \cdot 2\text{H}_2\text{O}$  (43 mg, 0.234 mmol dissolved in 3 mL of MeOH) was added. The progress of metal insertion was followed by UV-Vis spectroscopy (Soret and Q visible band changes). After 1 h of stirring at room temperature, the complex was quantitatively formed and obtained as a cherry-purple solid after solvent evaporation. Pure purple crystals of the desired compound was obtained after crystallization from  $\text{CHCl}_3/n$ -pentane (93 mg, 0.114 mmol; 96% yield). UV-Vis (THF):  $\lambda_{\text{max}}$  ( $\epsilon$ ,  $\text{M}^{-1} \text{cm}^{-1}$ ) = 424 (451,000), 556 (15,500), 595 (5,600) nm.  $^1\text{H}$  NMR (300 MHz, THF- $d_8$ ): 8.83 (m, 8 H,  $\beta$ -pyrr), 8.21 (m, 4H, ArH), 8.19 (m, 6H, ArH), 7.76 (m, 3H, ArH), 7.65 (m, 6H, ArH), 3.99 (m, 1 H, proline  $\alpha$ -H), 3.89 (m, 2 H, proline  $\delta$ -H), 2.34 (m, 2 H, proline  $\beta$ -H), 2.18 (m, 2 H, proline  $\gamma$ -H). FAB-MS (NBA), *m/z*: 818  $[\text{M}]^+$

### Determination of Enantiomeric Purity of (D)- and (L) $\text{ZnP}(-)$

The enantiomeric purity of (D) $\text{ZnP}(-)$  and (L) $\text{ZnP}(-)$  was checked by HPLC chromatography on a chiral stationary phase (c.s.p.), a method which has proved to be efficient for enantioseparation of chiral tetrapyrrole macrocycles (Belviso et al., 2018a,b). Accordingly, the racemic mixture and the two enantiomers were eluted on amylose tris(3,5-dimethylphenylcarbamate) c.s.p. This c.s.p. allowed separation of the racemic mixture into the two enantiomers (D) $\text{ZnP}(-)$  and (L) $\text{ZnP}(-)$  (see **Supplementary Figure 4**) even if a peak overlap occurs as a consequence of a peak tailing probably due to aggregation phenomena in the required elution mixture. In particular, (L) $\text{ZnP}(-)$  showed a retention time of 28.90 min, while (D) $\text{ZnP}(-)$  a retention time of 36.70 min. Comparison of the racemic mixture chromatogram with those of the single enantiomers allowed to establish that both samples were enantiomerically pure, showing no traces of the other stereoisomer.

### Aggregation Studies

All the spectroscopic studies have been carried out at 298 K. Solutions suitable for the aggregation studies were prepared as follows. Porphyrin stock solutions in ethanol (ca.  $10^{-4}$  M concentration) were gently warmed, then briefly sonicated and finally filtered through a 0.22  $\mu\text{m}$  Nylon<sup>®</sup> membrane (Hahnem $\ddot{A}$ 1/4le Albet<sup>®</sup> Syringe Filters), prior to use. These precautions have been taken to avoid uncontrolled nucleation of porphyrin protoaggregates that would affect the reproducibility of the experiments. Check of the effective concentration was made by UV-Vis spectroscopy in pure ethanol (Soret band intensity of the porphyrins in monomeric form;  $\epsilon = 4.51 \times 10^5 \text{ M}^{-1} \text{cm}^{-1}$ ). Aggregation of title porphyrins has been carried out in aqueous ethanol solutions (EtOH/ $\text{H}_2\text{O}$  25:75 v:v; 298 K) at 1, 5 and 10  $\mu\text{M}$  concentration, by strictly following a "porphyrin first" protocol. Namely, a proper aliquot of a stock solution of porphyrin (10–100  $\mu\text{L}$ ), was added to the required amount of ethanol (final volume of 1.0 mL) in an 8 mL glass vial, and briefly sonicated. To this solution 3.0 mL of water were then slowly added, again under sonication, to give 4.0 mL of resulting solution with 25% v:v solvent proportion, with the required porphyrin concentration. A ca.

2.5 mL portion was finally transferred into a quartz cuvette and the relative spectra were then acquired at different time in order to monitoring the temporal evolution of the systems. This second sonication step appears to be of crucial importance for a good reproducibility of the results, that depends on the homogeneity of the morphology of the initially formed porphyrin clusters, which would be detrimentally affected by the unavoidable occurrence of both gradient of concentration and solvent polarity changes, during the mixing with water. The porphyrin stock solutions should be used within 2 weeks from preparation, to ensure optimal reproducibility of the results.

## Kinetic Studies

Kinetic studies on the aggregation process of the title porphyrins, have been carried out in EtOH/H<sub>2</sub>O (75:25 v:v) and followed by CD spectroscopy. In all of the case examined, the first aggregation stage (Type-I aggregate formation) was in general too fast to be followed by conventional spectroscopic techniques. As far as the second process is concerned (Type-II aggregate formation) autocatalytic-type behavior of the molar ellipticity [ $\theta$ ] vs. time profiles have been obtained. The experimental data have been fitted by the Equation 1, reported in the Results and Discussion section of the text. The kinetic parameters were obtained by non-linear regression fit (KaleidaGraph 4.1, Synergy Software, 2011), over tens of data points. Entry values of  $k$  and  $n$  were initially obtained by running the program with fixed initial and equilibrium experimental values (theta molar or extinction). Final regressions were operated with “free” initial and final parameters to give final calculated values, that have been found to be always in good agreement with the experimental ones. The final kinetic data, reported in **Table 1**, are the averaged values obtained over at least three different runs, and for both minimum and maximum wavelength of lower

energy, most intense coupled bands at 436 and 443 nm, of the CD spectra.

## DATA AVAILABILITY STATEMENT

The original contributions presented in the study are included in the article/**Supplementary Material**, further inquiries can be directed to the corresponding author/s.

## AUTHOR CONTRIBUTIONS

DM contributed to conception and design of the study. MSt synthesized the title porphyrins. FZ performed SEM characterization of samples. DM, GMag, and MSa performed the Circular Dichroism measurements. MSa and MV performed the fluorescence spectroscopy studies. SB, GMar, and SS performed chiral HPLC analysis. DM organized the database and performed the fitting and statistical analysis. GMag performed the editing of the figures and plots. MSt, DM, MV, CD, SS, and RP wrote sections of the manuscript. RP was responsible for the financial support to the work. All authors contributed to the discussion and interpretation of the results and to manuscript revision, and read and approved the submitted version.

## FUNDING

This research was funded by the European Community, H2020-FETOPEN, 828779, INITIO project.

## SUPPLEMENTARY MATERIAL

The Supplementary Material for this article can be found online at: <https://www.frontiersin.org/articles/10.3389/fchem.2020.587842/full#supplementary-material>

## REFERENCES

- Arteaga, O., El-Hachemi, Z., Canillas, A., Crusats, J., Rovira, M., and Ribó, J. M. (2016). Reversible and irreversible emergence of chiroptical signals in J-aggregates of achiral 4-sulfonatophenyl substituted porphyrins: intrinsic chirality vs. chiral ordering in the solution. *Chem. Commun.* 52, 10874–10877. doi: 10.1039/C6CC005709H
- Belviso, S., Capasso, S., Santoro, E., Najafi, L., Lelj, F., Superchi, S., et al. (2018a). Thioethyl-porphyrazine/nanocarbon hybrids for photoinduced electron transfer. *Adv. Funct. Mater.* 28, 1705418. doi: 10.1002/adfm.201705418
- Belviso, S., Santoro, E., Lelj, F., Casarini, D., Villani, C., Franzini, R., et al. (2018b). Stereochemical stability and absolute configuration of atropisomeric thioalkylporphyrazines by dynamic NMR and HPLC studies and computational analysis of HPLC-ECD recorded spectra. *Eur. J. Org. Chem.* 4029–4037. doi: 10.1002/ejoc.201800553
- Berova, N., Di Bari, L., and Pescitelli, G. (2007). Application of electronic circular dichroism in configurational and conformational analysis of organic compounds. *Chem. Soc. Rev.* 36, 914–931. doi: 10.1039/b515476f
- Berova, N., Nakanishi, K., and Woody, R. W. (2000). *Circular Dichroism: Principles and Applications*, 2nd Edn. Weinheim: Wiley-WCH.
- Borovkov, V. V., Harada, T., Hembury, G. A., and Inoue, Y. (2003). Solid-state supramolecular chirogenesis: high optical activity and gradual development of zinc octaethylporphyrin aggregates. *Angew. Chem. Int. Ed.* 42, 1746–1749. doi: 10.1002/anie.200250524
- Borovkov, V. V., and Inoue, Y. (2006). Supramolecular chirogenesis in host-guest systems containing porphyrinoids. *Top. Curr. Chem.* 265, 89–146. doi: 10.1007/128\_037
- Borovkov, V. V., Lintuluoto, J. M., Fujiki, M., and Inoue, Y. (2000). Temperature effect on supramolecular chirality induction in bis(zinc porphyrin). *J. Am. Chem. Soc.* 122, 4403–4407. doi: 10.1021/ja9936971
- Borovkov, V. V., Lintuluoto, J. M., and Inoue, Y. (2001). Supramolecular Chirogenesis in zinc porphyrins: mechanism, role of guest structure, and application for the absolute configuration determination. *J. Am. Chem. Soc.* 123, 2979–2989. doi: 10.1021/ja0032982
- Caroleo, F., Stefanelli, M., Magna, G., Venanzi, M., Paolesse, R., Sennato, S., et al. (2019). Kinetic and spectroscopic studies on the chiral self-aggregation of amphiphilic zinc and copper (L)-prolinato-tetraarylporphyrin derivatives in different aqueous media. *Org. Biomol. Chem.* 17, 1113–1120. doi: 10.1039/C8OB02689K
- Caruso, M., Gatto, E., Mazzuca, C., Stella, L., Bocchinfuso, G., Palleschi, A., et al. (2013). Fibrils or globules? Tuning the morphology of peptide aggregates from helical building blocks. *J. Phys. Chem. B* 117, 5448–5459. doi: 10.1021/jp400009j
- Castriciano, M. A., Romeo, A., De Luca, G., Villari, V., Monsù Scolaro, L., and Micali, N. (2011). Scaling the chirality in porphyrin J-nanoaggregates. *J. Am. Chem. Soc.* 133, 765–767. doi: 10.1021/ja110028g
- Castriciano, M. A., Romeo, A., Zagami, R., and Micali, N. (2012). Kinetic effects of tartaric acid on the growth of chiral J-aggregates of

- tetrakis(4-sulfonatophenyl)porphyrin. *Chem. Commun.* 48, 48722–48724. doi: 10.1039/c2cc00028h
- Chen, P., Ma, X., Hu, K., Rong, Y., and Liu, M. (2011). Left or right? The direction of compression-generated vortex-like flow selects the macroscopic chirality of interfacial molecular assemblies. *Chem. Eur. J.* 17, 12108–12114. doi: 10.1002/chem.201101322
- Cui, L., Tokarz, D., Cisek, R., Ng, K. K., Wang, F., Chen, J., et al. (2015). Organized aggregation of porphyrins in lipid bilayers for third harmonic generation microscopy. *Angew. Chem. Int. Ed.* 54, 13928–13932. doi: 10.1002/anie.201506171
- D'Urso, A., Fragalà, M. E., and Purrello, R. (2012). From self-assembly to noncovalent synthesis of programmable porphyrins' arrays in aqueous solution. *Chem. Commun.* 48, 8165–8176. doi: 10.1039/c2cc31856c
- El-Hachemi, Z., Balaban, T. S., Campos, J. L., Cespedes, S., Crusats, J., Escudero, C., et al. (2016). Effects of hydrodynamic forces on meso-(4-sulfonatophenyl)-substituted porphyrin J-aggregate nanoparticles: elasticity, plasticity and breaking. *Chem. Eur. J.* 22, 9740–9749. doi: 10.1002/chem.201600874
- El-Hachemi, Z., Escudero, C., Arteaga, O., Canillas, A., Crusats, J., Mancini, G., et al. (2009). Chiral sign selection on the J-aggregates of deprotonated tetrakis(4-sulfonatophenyl)porphyrin by traces of unidentified chiral contaminants present in the ultra-pure water used as solvent. *Chirality* 21, 408–412. doi: 10.1002/chir.20602
- El-Hachemi, Z., Mancini, G., Ribó, J. M., and Sorrenti, A. (2008). Role of the hydrophobic effect in the transfer of chirality from molecules to complex systems: from chiral surfactants to porphyrin/surfactant aggregates. *J. Am. Chem. Soc.* 130, 15176–15184. doi: 10.1021/ja805669v
- Feldborg, L. N., Saletta, W. J., Iavicoli, P., and Amabilino, D. B. (2011). Central metal ion determined self-assembly of intrinsically chiral porphyrins. *J. Porphyrins Phthalocyanines* 15, 995–1003. doi: 10.1142/S108842461100394X
- Guijarro, A., and Yus, M. (2009). *The Origin of Chirality in the Molecules of Life*. Cambridge: RSC Publishing.
- Intrieri, D., Damiano, C., Rizzato, S., Paolesse, R., Venanzi, M., Monti, D., et al. (2018). Sensing of diclofenac by a porphyrin-based artificial receptor. *New J. Chem.* 42, 15778–15783. doi: 10.1039/C8NJ02737D
- Labuta, J., Hill, J. P., Ishihara, S., Hanykova, L., and Ariga, K. (2015). Chiral sensing by nonchiral tetrapyrroles. *Acc. Chem. Res.* 48, 521–259. doi: 10.1021/acs.accounts.5b00005
- Lee, H., Hong, K.-I., and Jang, W.-D. (2018). Design and applications of molecular probes containing porphyrin derivatives. *Coord. Chem. Rev.* 354, 46–73. doi: 10.1016/j.ccr.2017.06.008
- Liu, M., Zhang, L., and Wang, T. (2015). Supramolecular chirality in self-assembled systems. *Chem. Rev.* 115, 7304–7397. doi: 10.1021/cr500671p
- Lorecchio, C., Venanzi, M., Mazzuca, C., Lettieri, R., Palleschi, A., Thi, T. H. N., et al. (2014). Tuning the chiroptical and morphological properties of steroidal-porphyrin aggregates: a mechanistic, structural, and MM investigation. *Org. Biomol. Chem.* 12, 3956–3963. doi: 10.1039/C4OB00134F
- Magna, G., Monti, D., Di Natale, C., Paolesse, R., and Stefanelli, M. (2019). The assembly of porphyrin systems in well-defined nanostructures: an update. *Molecules* 24:4307. doi: 10.3390/molecules24234307
- Mathew, S. P., Iwamura, H., and Blackmond, D. G. (2004). Amplification of enantiomeric excess in a proline-mediated reaction. *Angew. Chem. Int. Ed.* 43, 3317–3321. doi: 10.1002/anie.200453997
- Micali, N., Engelkamp, H., van Rhee, P. G., Christianen, P. C. M., Monsù Scolaro, L., and Maan, J. C. (2012). Selection of supramolecular chirality by application of rotational and magnetic forces. *Nat. Chem.* 4, 201–207. doi: 10.1038/nchem.1264
- Micali, N., Mallamace, F., Castriciano, M., Romeo, A., and Monsù Scolaro, L. (2001). Separation of scattering and absorption contributions in UV/Visible spectra of resonant systems. *Anal. Chem.* 73, 4958–4963. doi: 10.1021/ac010379n
- Micali, N., Mallamace, F., Romeo, A., Purrello, R., and Monsù Scolaro, L. (2000). Mesoscopic structure of meso-tetrakis(4-sulfonatophenyl)porphyrin J-aggregates. *J. Phys. Chem. B* 104, 5897–5904. doi: 10.1021/jp991909a
- Micali, N., Villari, V., Castriciano, M. A., Romeo, A., and Monsù Scolaro, L. (2006). From fractal to nanorod porphyrin J-aggregates. Concentration-induced tuning of the aggregate size. *J. Phys. Chem. B* 110, 8289–8295. doi: 10.1021/jp060730e
- Monsù Scolaro, L., Castriciano, M., Romeo, A., Mazzaglia, A., Mallamace, F., and Micali, N. (2002). Nucleation effects in the aggregation of water-soluble porphyrin aqueous solutions. *Physica A* 304, 158–169. doi: 10.1016/S0378-4371(01)00547-7
- Monti, D. (2014). Recent advancements in chiral porphyrin self-assembly. *Top. Heterocycl. Chem.* 33, 231–292. doi: 10.1007/7081\_2013\_110
- Monti, D., De Rossi, M., Sorrenti, A., Laguzzi, G., Gatto, E., Stefanelli, M., et al. (2010). Supramolecular Chirality in solvent-promoted aggregation of amphiphilic porphyrin derivatives: kinetic studies and comparison between solution behavior and solid-state morphology by AFM topography. *Chem. Eur. J.* 16, 860–870. doi: 10.1002/chem.200901964
- Ohno, O., Kaizu, Y., and Kobayashi, H. (1993). J-aggregate formation of a water-soluble porphyrin in acidic aqueous media. *J. Chem. Phys.* 99, 4128–4139. doi: 10.1063/1.466109
- Oliveira-González, C., Di Meo, F., González-Campo, A., Beljonne, D., Norman, P., Simeón-Sorbed, M., et al. (2015). Bottom-up hierarchical self-assembly of chiral porphyrins through hydrogen bonds. *J. Am. Chem. Soc.* 137, 15795–15808. doi: 10.1021/jacs.5b08081
- Paolesse, R., Monti, D., Dini, F., and Di Natale, C. (2011). Fluorescence based sensor arrays. *Top. Curr. Chem.* 300, 139–174. doi: 10.1007/128\_2010\_97
- Paolesse, R., Nardis, S., Monti, D., Stefanelli, M., and Di Natale, C. (2017). Porphyrinoids for chemical sensor applications. *Chem. Rev.* 117, 2517–2583. doi: 10.1021/acs.chemrev.6b00361
- Pasternack, R., Gibbs, E. J., Bruzewicz, D., Stewart, D., and Engstrom, K. S. (2002). Kinetics of disassembly of a DNA-bound porphyrin supramolecular array. *J. Am. Chem. Soc.* 124, 3533–3539. doi: 10.1021/ja01124820
- Pasternack, R. F., Bustamante, C., Collings, P. J., Giannetto, A., and Gibbs, E. J. (1993). Porphyrin assemblies on DNA as studied by a Resonance Light-Scattering technique. *J. Am. Chem. Soc.* 115, 5393–5399. doi: 10.1021/ja00066a006
- Pasternack, R. F., Fleming, C., Herring, S., Collings, P. J., dePaula, J., DeCastro, G., et al. (2000). Aggregation kinetics of extended porphyrins and cyanine dyes assemblies. *Biophys. J.* 79, 550–560. doi: 10.1016/S0006-3495(00)76316-8
- Romeo, A., Castriciano, M. A., Occhiuto, I., Zagami, R., Pasternack, R. F., and Monsù Scolaro, L. (2014). Kinetic control of chirality in porphyrin J-aggregates. *J. Am. Chem. Soc.* 136, 40–43. doi: 10.1021/ja410514k
- Simoncini, E., Caroleo, F., Ceccacci, F., Mancini, G., Stefanelli, M., Paolesse, R., et al. (2014). Surfactant-induced chirality on reluctant aggregates of a chiral amphiphilic cationic (L)-proline-Zn(II)porphyrin conjugate in water. *RSC Adv.* 4, 55362–55366. doi: 10.1039/C4RA05870D
- Sorrenti, A., El-Hachemi, Z., Arteaga, O., Canillas, A., Crusats, J., and Ribó, J. M. (2012). Kinetic control of the supramolecular chirality of porphyrin J-aggregates. *Chem. Eur. J.* 18, 8820–8826. doi: 10.1002/chem.201200881
- Sorrenti, A., Rodriguez-Trujillo, R., Amabilino, D. B., and Puigmartí-Luis, J. (2016). Milliseconds make the difference in far-from-equilibrium self-assembly of supramolecular chiral nanostructures. *J. Am. Chem. Soc.* 138, 6920–6923. doi: 10.1021/jacs.6b02538
- Stefanelli, M., Magna, G., Zurlo, F., Caso, F. M., Di Bartolomeo, E., Antonaroli, S., et al. (2019). Chiral selectivity of porphyrin-ZnO nanoparticle conjugates. *ACS Appl. Mater. Interfaces.* 11, 12077–12087. doi: 10.1021/acsami.8b22749
- Valev, V. K., Baumberg, J. J., De Clercq, B., Braz, N., Zheng, X., Osley, E. J., et al. (2014). Nonlinear superchiral meta-surfaces: tuning chirality and disentangling non-reciprocity at the nanoscale. *Adv. Mater.* 26, 4074–4081. doi: 10.1002/adma.201401021
- van der Weegen, R., Teunissen, A. J. P., and Meijer, E. W. (2017). Directing the self-assembly behavior of porphyrin-based supramolecular systems. *Chem. Eur. J.* 23, 3773–3783. doi: 10.1002/chem.201605872
- Wang, Y., Xu, J., Wang, Y., and Chen, H. (2013). Emerging chirality in nanoscience. *Chem. Soc. Rev.* 42, 2930–2962. doi: 10.1039/C2CS35332F
- Yoon, M., Srirambalaji, R., and Kim, K. (2012). Homochiral metal-organic frameworks for asymmetric heterogeneous catalysis. *Chem. Rev.* 112, 1196–1231. doi: 10.1021/cr2003147
- Zelenka, K., Trnka, T., Tislerová, I., Monti, D., Cinti, S., Naitana, M. L., et al. (2011). Spectroscopic, morphological, and mechanistic investigation of the solvent-promoted aggregation of porphyrins modified in meso-positions by glucosylated steroids. *Chem. Eur. J.* 17, 13743–13753. doi: 10.1002/chem.201101163

Zhou, C., Feng, X., Wang, R., Yang, G., Wang, T., and Jiang, J. (2018). Hierarchical assembly of L-phenylalanine-terminated bolaamphiphile with porphyrin show tunable nanostructures and photocatalytic properties. *ACS Omega* 3, 10638–10646. doi: 10.1021/acsomega.8b01822

**Conflict of Interest:** The authors declare that the research was conducted in the absence of any commercial or financial relationships that could be construed as a potential conflict of interest.

*Copyright © 2020 Stefanelli, Savioli, Zurlo, Magna, Belviso, Marsico, Superchi, Venanzi, Di Natale, Paolesse and Monti. This is an open-access article distributed under the terms of the Creative Commons Attribution License (CC BY). The use, distribution or reproduction in other forums is permitted, provided the original author(s) and the copyright owner(s) are credited and that the original publication in this journal is cited, in accordance with accepted academic practice. No use, distribution or reproduction is permitted which does not comply with these terms.*